Finite Element mesh coarsening for effective distortion prediction in Wire Arc Additive Manufacturing

Title: Finite Element mesh coarsening for effective distortion prediction in Wire Arc Additive Manufacturing

Authors: Filippo Montevecchi, Giuseppe Venturini, Niccolò Grossi, Antonio Scippa, Gianni Campatelli

DOI: https://doi.org/10.1016/j.addma.2017.10.010
Reference: ADDMA 231

To appear in:

Received date: 07/11/2016
Revised date: 28/09/2017
Accepted date: 08/10/2017

Please cite this article as: Filippo Montevecchi, Giuseppe Venturini, Niccolò Grossi, Antonio Scippa, Gianni Campatelli, Finite Element mesh coarsening for effective distortion prediction in Wire Arc Additive Manufacturing (2017), https://doi.org/10.1016/j.addma.2017.10.010

Title
Finite Element mesh coarsening for effective distortion prediction in Wire Arc Additive Manufacturing

Authors
Filippo Montevecchi[a*], Giuseppe Venturini[a], Niccolò Grossi[a], Antonio Scippa[a], Gianni Campatelli[a]

[a] *Affiliation*: Department of Industrial Engineering, University of Firenze, Via di Santa Marta 3, Firenze, 50139, Italy.

**Corresponding author*: Tel.: +39-055-2758726. E-mail address: filippo.montevecchi@unifi.it

Abstract
WAAM (Wire Arc Additive Manufacturing) is a metal AM (Additive Manufacturing) technology that allows high deposition rates and the manufacturability of very large components, compared to other AM technologies. Distortions and residual stresses affecting the manufactured parts represent the main drawbacks of this AM technique. FE (Finite Element) modeling could represent an effective tool to tackle such issues, since it can be used to optimize process parameters, deposition paths and to test alternative mitigation strategies. Nevertheless, specific modeling strategies are needed to reduce the computational cost of the process simulation, such as reducing the number of elements used in discretizing the model. This paper presents an alternative technique to reduce the number of elements required to discretize the substrates of WAAM workpieces. The proposed technique is based on dividing the substrate in several zones, separately discretized and then connected by means of a double sided contact algorithm. This strategy allows to achieve a significant reduction of the number of elements required, without affecting their quality parameters. The geometry and dimension of the mesh zones are identified through a dedicated algorithm that allows to achieve an accurate temperature prediction with the minimum element number. The effectiveness of the proposed technique was tested by means of both numerical and experimental validation tests.

Keywords:
Wire-Arc-Additive-Manufacturing, Gas-Metal-Arc-Welding, Finite Element.

1. INTRODUCTION

Among metal AM (Additive Manufacturing) processes, WAAM (Wire Arc Additive Manufacturing) appears to be one of the most interesting in terms of achievable material deposition rates and maximum part size [1]. WAAM is a DED (Direct Energy Deposition) technology, i.e., a metal AM technique in which the component layers are created by selective deposition of molten metal. In WAAM, the added metal is deposited using arc welding techniques such as GMAW (Gas Metal Arc Welding), GTAW (Gas Tungsten Arc Weld- ing) or PAW (Plasma Arc Welding) [2].
The components manufactured by WAAM are prone to residual stresses and distortion issues [3]. It should be pointed out that such criticalities affect all metal AM technologies, since they are caused by the non-uniform temperature field in the part during the manufacturing process. Simulations provide an effective tool to investigate the main leverages to mitigate or compensate such issues, allowing to test process improvement in a cost and time effective way. The effectiveness of process simulation has been proven in several works: Denlinger and Michaleris [4] used FE modeling to develop a distortions compensation strategy tailored for AM of large parts and to investigate the effect of stress relaxation on part displacements and residual stresses [5]. Salonitis et al. [6] studied the interaction of direct laser deposition AM and post-process milling to determine the actual residual stresses after the finishing process. The simulation of AM processes is usually carried out in analogy to the techniques used in multi-pass welding simulations: basically, a transient thermo-mechanical FE analysis is carried out, simulating the heat transfer to the workpiece by means of an heat source model [7]. The material deposition is taken into account by including specific algorithms that activate the bead elements according to the deposition process [8].
Despite the accuracy and effectiveness achievable by FE process modeling, a significant drawback of such technique is the high computational cost associated with the large model size and the high

number of simulation steps required. Since AM simulations are performed via transient analyses, two main paths could be followed to improve the simulation time efficiency: reducing the number of simulation steps and reducing FE model DOFs (Degrees Of Freedom). The most effective approach to reduce the number of simulation steps was presented by Ding et al. ([9,10]) that proposed to treat both the heat transfer and the mechanical domains as steady state problems in a reference frame moving according to the deposition path. This strategy requires a single simulation step to be performed for each component layer, resulting in a significant reduction of computation time. However, this approach returns accurate results only on large components, since the steady state approximation introduces significant errors for reduced part size [11]. Therefore, for an effective reduction of simulation time in arbitrary part size, it is crucial to develop techniques focusing on the reduction of FE model DOFs. This paper deals with this aspect, aiming at improving AM simulation efficiency.

In an AM simulation model, the number of elements (i.e., the number of DOFs), is constrained by the maximum mesh size required by the molten pool. Indeed, since metal deposition involves a local heating of the workpiece, to achieve an accurate description of the temperature field, a minimum number of elements per molten pool radius must be used. This aspect was already shown in the simulation of similar processes, such as welding [12], and laser forming [13]. Such requirement leads to a constraint for the elements size of both filler material and substrate. In particular, all the FE elements representing the deposited material should meet the maximum size criterion, because during the simulation they will experience a melting transformation. Nevertheless, one should consider that this requirement needs to be met locally, where the molten pool induces relevant temperature gradients. It is worth noting that, as the simulation progresses, the deposition head and consequently the molten pool move along the substrate. This leads to filler regions represented by a number of elements, originally defined in accordance with the maximum size criterion, that would result excessive, considering the reduction of temperature gradients over those areas. In addition, the substrate elements size shall be defined in accordance to the one of the filler (to ensure mesh connectivity) even though the substrate will not experience any phase change.

Considering these aspects, the techniques to reduce the model DOFs pursue two main strategies: i) reducing the number of elements of the filler metal far from the molten pool and ii) reducing the number of elements of the substrate. In the first group, an adaptive re-meshing of the deposited material elements is performed. Denlinger et al. [14] presented a re-meshing technique in which a mesh coarsening is performed after the deposition of every layer, extracting solution variables on the coarsened grid by means of an interpolation algorithm. In AM simulation, the most common technique to reduce the elements of the substrate is mesh-biasing [15], in which the substrate mesh size is increased proportionally to the distance from the filler elements. This technique is adopted in most AM FE simulations, but it shows a significant drawback: an excessive increase in mesh size could affect elements geometry, leading to the generation of elements with excessive aspect ratios [16]. This can lead to severe issues in the mechanical analysis, introducing errors in estimating the base material bending [17].

This paper presents a new method to reduce the number of elements required for the substrate discretization. Unlike the traditional mesh biasing technique, the proposed approach increases the elements size without affecting the elements quality. This is achieved by splitting the substrate geometry in multiple sections that are discretized individually with different mesh size. The model of the complete substrate is then created by connecting the different sections with a double sided contact algorithm. The details of the proposed technique will be discussed in Section 2. In Section 3 a numerical validation is presented: a simple bead on plate simulation is carried out using the proposed mesh coarsening technique and the results in terms of temperature distribution are compared with a reference model. In Section 4 both the mesh biasing and the proposed technique are applied to an experimental case study, comparing the actual and simulated distortions. This validation allowed to prove the accuracy of the proposed modeling technique, in terms of distortions prediction, which, together with the reduced computational time, paves the way to the adoption of suitable optimization approaches [18], to mitigate such criticality.

2. Proposed method

The residual stresses and distortions of AM parts are related to the non-uniform temperature distribution in the workpiece. For this reason, thermo-mechanical coupled FE models are used to model such effects in AM operations.
Since the outcome of the heat transfer analysis (transient temperature distribution of the workpiece) is used as input load for the mechanical analysis, correctly capturing the temperature gradients in this phase is mandatory to ensure an accurate prediction of the workpiece mechanical response. Hence, the FE mesh pattern and size must be consistent with temperature gradients experienced by the workpiece, conflicting with the need of reducing the simulation time, usually achieved by reducing the number of elements.
The proposed method allows to reduce the number of FE elements used to discretize the workpiece, without introducing significant errors in estimating the temperature field. The base concept is to replace the mesh biasing technique with a mesh zoning approach, which consists in defining different zones of the work- piece substrate to be separately discretized and then connected in order to achieve a continuous body behavior. Hence, the workpiece is discretized with a discontinuous mesh, achieving a significant reduction of the elements number without compromising their aspect ratios and the results. The key points of proposed technique are:

1. Mesh zones joining.
2. Mesh zones definition.

2.1 Mesh zones joining

Varying the mesh size throughout the substrate geometry is a common practice to reduce the number of elements used for the discretization. This is usually performed with the mesh biasing technique, i.e., the element dimension is progressively increased in a specific direction to reduce the number of elements. This leads to a non-uniform mesh size, increasing with the distance from the filler material. An example of a biased mesh is shown in Fig. 1b.
Despite the straightforward implementation of such technique in the commercial FE pre-processors, it has a significant drawback: as the distance from the substrate increases, the element geometry experiences significant distortions, leading to high aspect ratio values, as exemplified in Fig. 1b. It is worth highlighting that this issue gets particularly relevant in hexahedral elements, while tetrahedrons better suite a biased mesh pattern without relevantly affecting the elements aspect ratio. On the other hand, hexahedrons are the most common type of elements used in both AM and welding simulation since they allow to achieve a high accuracy in the mechanical analysis with first order shape functions, unlike tetrahedron elements. For this reason, the proposed mesh coarsening technique will be discussed referring to hexahedral elements, but the application to tetrahedral elements is feasible and straightforward.

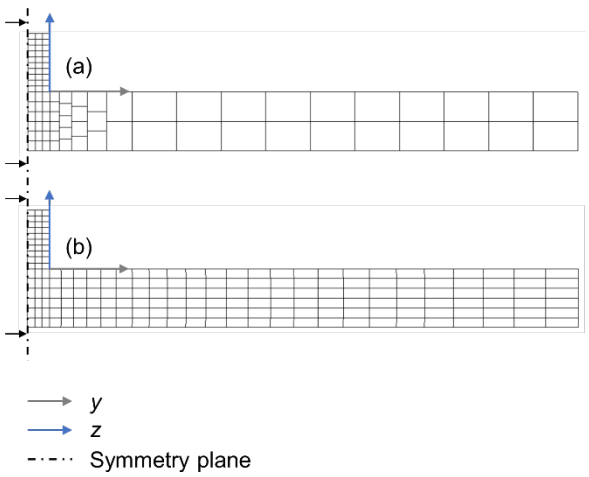

Fig. 1. Comparison of the proposed coarsening technique (a) and mesh biasing (b).

The proposed mesh zoning technique is based on a non-conformable interfaces approach. Indeed, the criticalities of the mesh biasing technique arise because the workpiece is discretized as a single body. This means that two adjacent zones with differ- ent mesh size, are forced to share the interface nodes, in order to provide structural continuity. The solution proposed to overcome such issue is based on discretizing the different zones separately, avoiding the conformable interface constraint, allowing the different zones to have different element size in both x, y and z directions, as exemplified in Fig. 1a. This gives the chance to fully exploit the mesh size identification algorithm, since the mesh size can be arbitrarily increased, without affecting the elements aspect ratios. This technique relies on joining the different zones in correspondence of non-conformable interfaces, to achieve the structural continuity, for both heat transfer and mechanical solutions. With the current FE solver capabilities this problem can be overcome by means of double sided contact algorithms, implemented in most commercial FE solvers and currently used for research purposes in several fields [19–21]. Indeed, for the mechanical solution these contact algorithms prescribe a set of multi-point-constraints blocking the relative motion of the interface in both normal and tangential directions. For the heat transfer solution, such algorithms enforce the contacting surfaces to have the same temperature and heat flux in normal direction. The mechanical and thermal constraints allow to simulate the behavior of a continuous body without requiring mesh conformity between the adjacent zones. Hence the double sided contact algorithm represents an effective tool to implement the mesh size distribution identified by the proposed algorithm, with- out resulting in a relevant increase of the elements aspect ratios over the zones further from the welding bead.

2.2. Mesh zones definition

Having highlighted the double sided contact algorithm as a key tool to balance model DOFs reduction and elements quality, identifying a suitable strategy to define the different mesh zones is mandatory. Indeed, the proposed mesh zoning involves an increase of mesh size, potentially affecting the solution accuracy. For this reason, a systematic tool to define the mesh zones pattern is thus proposed.

The FE models used for AM simulation can be divided in two main regions, featuring different requirements in terms of mesh size: the deposited material and the base material, on which this paper is focused. Different phenomena occur in such areas, requir- ing the adoption of different mesh sizing criteria. For what concerns the deposited material, the mesh size requirement is imposed by the dimension of the molten pool, i.e., to the heat source dimensions ([12,16]). On the opposite, the base material does not undergo the heat generation, exception made for the region underneath the first layer. Therefore, a different discretization requirement shall be identified for the substrate, to balance simulation accuracy and time efficiency.

The proposed technique allows to identify the mesh size required to effectively take into account the thermal gradients in the substrate and to implement such discretization, minimizing FE elements distortion. The concept is based on the fact that the exact value of the solution can be computed only at nodal points, when using the FE method to solve a heat transfer problem. In the remaining part of the domain, the solution variables are interpolated by means of FE elements shape functions [22]. Hence, the FE mesh should be defined consistently with the expected temperature field in order to minimize the interpolation error.

In practice, the proposed method starts with the estimation of the temperature distribution pattern by means of an approximated analytical solution of the heat transfer problem in welding. Then, such solution is fitted with a piecewise polynomial function. This interpolation process is similar to a FE solution, in which exact temperature values could be computed only in correspondence of mesh nodes. This allows to identify the largest mesh size, ensuring reduced error values.

The key aspects of the proposed method are:

- Analytical solution to estimate temperature distribution;
- Zone subdivision strategy;
- Zones mesh size definition;

2.2.1. Analytical solution

In this paper, the Rosenthal analytical solution is used to estimate the temperature field on the component substrate [23]. This simplified model allows to compute the workpiece temperature field, on the following assumptions:

- Punctual heat source, rather than a distributed one.
- Semi-infinite solid.
- The temperature dependence of material properties is neglected. • The transformation heat effect is neglected
- Straight welding trajectory.
- Quasi steady state solution.
-

The quasi steady state condition means that the workpiece has an infinite heat capacity, since it is assumed to be a semi-infinite solid. This allows treating the heat diffusion problem as steady state in a coordinate system moving according to the welding path, as defined in Eq. (1)

$$\begin{cases} x^1 = x - vt \\ y^1 = y \\ z^1 = y \end{cases} \quad \text{Eq. 1}$$

and shown in Fig. 2:

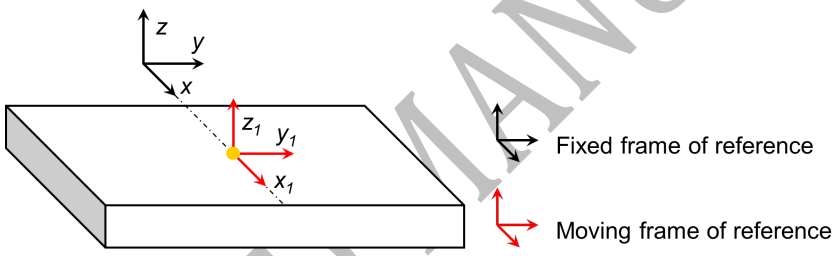

Fig. 2. Rosenthal model outline.

where v is the welding velocity. With these assumptions, the solution of the heat diffusion problem is given by Eq. (2):

$$T(x_1, y_1, z_1) = T_0 + \frac{\dot{Q}}{2\pi\lambda} \exp\left(-\frac{vx^1}{2\alpha}\right) \exp\left(-\frac{vR}{2\alpha}\right) \frac{1}{R} \quad \text{Eq. 2}$$

where T is the unknown temperature, T0 is the initial uniform work- piece temperature, □ is the thermal conductivity, □ is the thermal diffusivity, Q˙ is the thermal power input and R is defined by Eq. (3):

$$R = \sqrt{x_1^2 + y_1^2 + z_1^2} \quad \text{Eq. 3}$$

Clearly the Rosenthal model involves many strong assumptions, not ensuring an accurate estimation of the workpiece temperature field, in particular in correspondence of the molten region. Nevertheless, this model takes into account the most significant parameters of process and material, allowing to quickly provide an estimation of the temperature distribution over the workpiece for a specific configuration. Hence it is considered here a suitable aid for the definition the optimal mesh size.

2.2.2. Mesh pattern

A mesh pattern is required to achieve a mesh zoning of the work- piece substrate. In particular, a direction of mesh increase shall be selected. This paper proposes the mesh size increase along the y direction of the moving frame of reference defined by the Rosenthal model. The proposed mesh pattern is shown in Fig. 3 for a simple bead-on-plate: the substrate is divided into several zones, defined by selecting planes normal to the welding trajectory and to the substrate plane.

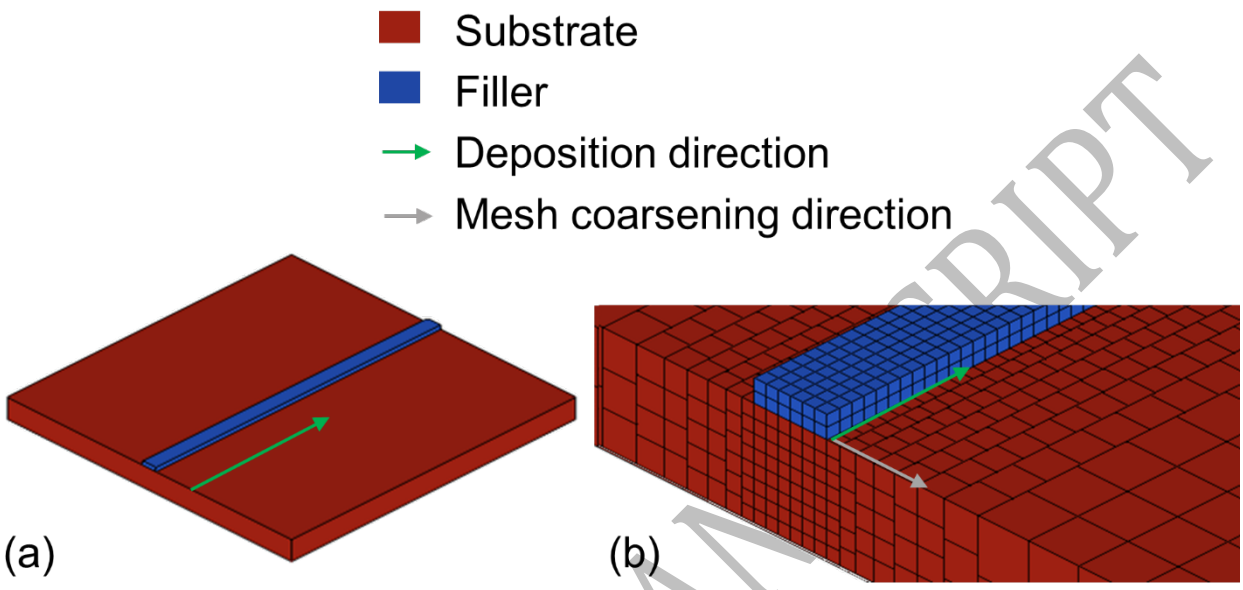

Fig. 3. Simple bead on plate geometry (a) modelled using mesh biasing (b) and the proposed technique (c).

Each zone is uniformly discretized by hexahedral elements: the zone underneath the welding bead meets the heat source mesh size constraints, while for the other zones the mesh size increases with the distance from the substrate. This is compliant with the Rosenthal temperature distribution pattern: as shown in Fig. 3 the temperature gradient is steeper in the proximity of the welding arc (i.e., of the molten pool) and experiences a significant decay at increasing distance from the arc center.

2.2.3. Mesh size identification algorithm

The key point of the mesh zoning strategy is to define the mesh size for every zone in order to meet the interpolation error requirements. This is achieved by means of a specific recursive algorithm that interpolates the analytical temperature distribution with a polynomial function of the same order of the shape functions used in the FE model. Since first order elements are most commonly adopted for the heat transfer analyses, the algorithm is here presented referring to this specific element order (i.e., linear interpolation function). For starters the analytical temperature distribution is calculated, given the welding and material parameters, as a function of the y coordinate only (i.e., the mesh coarsening direction). This is achieved by evaluating Eq. (2) in $x^1 = 0$, $y^1 = y$ and $z^1 = 0$, as shown in Eq. (4):

$$T(y) = T(0, y, 0) = \frac{\dot{Q}}{2\pi\lambda} exp\left(-\frac{vy}{2\alpha}\right)\frac{1}{y} \qquad \text{Eq. 4}$$

Eq. (4) represents a function of the y coordinate, describing the workpiece temperature profile for a specific welding operation. It must be pointed out that evaluating the T function at $x^1 = 0$ and $z^1 = 0$ is a conservative option, considering that the steepest temperature gradients in y direction are located onto the workpiece top surface, a finer interpolation is required to meet the error criterion.

Fig. 4a shows the zone partition obtained by the algorithm: each zone i has a lower bound marked as y^i_1 and an upper bound marked as y_2^i . Except for the lower bound of the zone 1, which coincides with the heat source semi-axis b, all the remaining boundaries are the unknowns to be identified. To achieve this, the algorithm operates in a sequential way, i.e., it identifies the unknown upper bound of a zone, which is used as the known lower bound of the subsequent. Fig. 4b outlines the identification procedure of the unknown boundary y_2^i.

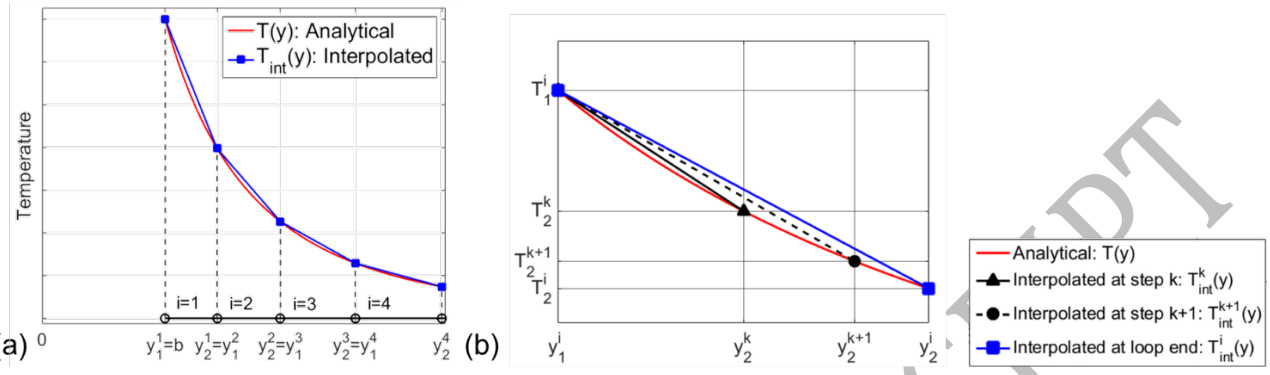

Fig. 4. Temperature profile interpolation through mesh zoning (a) and stepwise algorithm outline (b).

As shown in Fig. 4b, y_2^i is identified by means of a stepwise procedure. Assuming k parameter as step counter, a guess upper bound value is calculated, together with temperature values at zone boundary, as shown in Eq. (5):

$$\begin{cases} y_1^i = y_2^{i-1} \\ y_2^k = y_1^i + sk \\ T_1^i = T\left(y_1^i\right) \\ T_2^k = T\left(y_2^k\right) \end{cases} \quad \textbf{Eq. 5}$$

The parameter y_2^k is the guess upper bound of the *i*-th segment, T_1^i is the analytical temperature value computed in y_1^k and T_2^k is the analogous for y_2^k. The parameter *s* is the step distance, i.e., the distance between two subsequent guess boundaries. In order to ensure an accurate identification of the zones mesh size, *s* should be set to be much smaller than the heat source radius *b*. Once that guess zone boundaries are computed, the interpolation function is defined according to Eq. 6:

$$T_{int}^k(y) = \frac{T_2^k - T_1^i}{y_2^k - y_1^i}\left(y - y_1^i\right) + T_1^i \quad \textbf{Eq. 6}$$

This function represents the best approximation of the analytical temperature distribution achievable by a FE solver between the nodes placed in y_1^i and y_2^k (i.e., linear shape function). Finally, the interpolation error can be calculated using Eq. 7:

$$Err = max\left|\frac{T_{int}^k - T(y)}{T(y)}\right| \quad y \in \left[y_1^i \;\; y_2^k\right] \quad \textbf{Eq. 7}$$

The *Err* parameter, is the absolute maximum of the relative error between the analytical temperature distribution and its interpolation. Due to the complexity of the Rosenthal function, an analytical solution is hardly practicable and the most convenient way to identify it is by means of numerical techniques. Once the error value for the current guess is computed, the following check (Eq. 8) is performed:

$$Err \geq Err_t \quad \textbf{Eq. 8}$$

where Err_t is the target error value. Basically, this condition is the stopping criterion for the boundary search algorithm: as shown in **Error! Reference source not found.**b, if the *s* parameter is kept much smaller than *b*, the *Err* parameter will increase with the number of guesses, allowing to trigger the target error value, i.e., providing the maximum mesh size that allows to reach the required accuracy. If the stopping criterion is not met, then another guess is performed, calculating the zone upper bound as shown in Eq. 9:

$$y_2^{k-1} = y_1^i + (k+1)s \quad \textbf{Eq. 9}$$

Otherwise if the criterion is met, another zone will be analyzed, after the calculation of its lower bound and the mesh size for the current zone, according to Eq. 10 and Eq. 11:

$$y_1^{i+1} = y_2^i = y_2^k \quad \textbf{Eq. 10}$$

$$d_{el}^i = y_1^{i+1} - y_1^i \quad \textbf{Eq. 11}$$

It must be pointed out that the error parameter should not be regarded as the value of the expected discrepancy between the FE model and the experimental data. Such parameter represents the capability of a specific mesh to interpolate a reference temperature profile, hence its theoretical maximum precision to fit the theoretical temperature distribution.

3. Numerical validation

The proposed discretization technique was validated by means of a two-step approach: a numerical and an experimental one. The former was carried out to evaluate the accuracy of the proposed technique to predict the base plate temperature distribution, with respect to a reference model. On the other hand, the experimental validation was carried out to verify the effect of the achievable accuracy in temperature prediction on the mechanical calculation.
This section discusses the numerical validation: first the general modeling procedures used for both the numerical and experimental validation are presented, then the specific test case used for the numerical validation is introduced, discussing the results.

3.1. FE modeling description

In this section the modeling procedures used for the validation analyses are discussed, dealing with the following aspects:

- Heat source modeling
- Material deposition modeling
- Latent heat modeling

3.1.1. Heat source modeling

The state of the art heat source model for WAAM, is represented by the Goldak double ellipsoid [24]. In this paper, an alternative model developed by the authors [25], was chosen over the traditional double ellipsoid. As in the double ellipsoid model, the proposed heat source prescribes the welding heat input as a heat generation function, but it allows to control the amount of total power delivered to the substrate and to the filler. Indeed, in GMAW process, a part of the arc power is delivered directly to the substrate while the remaining part is consumed in melting the filler metal and then

transmitted to the workpiece by means of the molten filler droplets enthalpy [26]. As a first approximation, 50% of the total power is assumed to be delivered to the substrate and the remaining 50% to the filler metal [27]. Since the Goldak heat source prescribes a Gaussian distribution, achieving such power subdivision requires a tuning operation of the ellipsoid semi-axes dimensions, usually selected according to the molten pool dimen- sions. The proposed heat source layout is shown in Fig. 5.

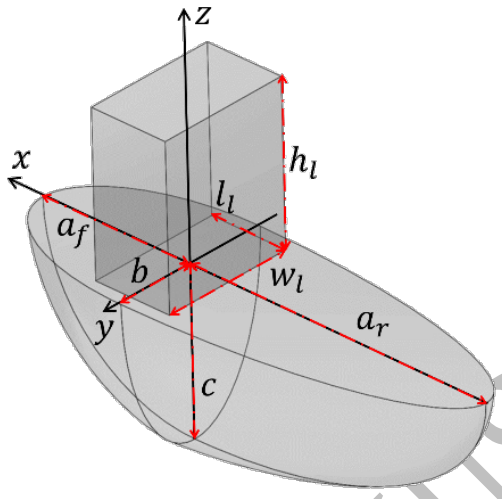

Fig. 5. Proposed heat source model.

The base metal heat input is delivered by a Goldak distribution, while the heat input to the filler metal is delivered by a constant power distribution. The proposed heat source is described by Eq. (12):

$$\begin{cases} \dot{q}_b = \dfrac{6\sqrt{3}\dot{Q}_b f_{f,r}}{\pi\sqrt{\pi}a_{f,r}bc}\exp\left[-3\left(\dfrac{x^2}{a_{f,r}^2}+\dfrac{y^2}{b^2}+\dfrac{z^2}{c^2}\right)\right] \\ \dot{q}_w = \dfrac{\dot{Q}_w}{V_{el}} \end{cases} \quad \text{Eq. 12}$$

where $\dot{q}_b$ and $\dot{q}_w$ are the power density functions for the base and the filler metal respectively, $\dot{Q}_b$ and $\dot{Q}_w$ are the corresponding power values, i.e., fractions of total electrical power. For both the filler and base metal, x, y and z represent the axes of a cartesian coordinate system moving according to the deposition path, as shown in Fig. 5. The $f_{f,r}$ terms in the base metal distribution, represent the distribution factor: subscript f,r means that these terms assume different values for x > 0 (front value f) and x < 0 (rear value r). The coefficients a, b and c are the semi-axes of an ellipsoidal surface representing the space region where the generated power density ($\dot{q}_v$) drops to the 5% of its peak value. Basically, the parameters of the base material heat source are the same used in the classic Goldak model [24].

The filler metal part of the heat source is defined as the ratio between the filler metal power and Vel, that is the volume of the currently heated elements. Indeed, for the filler metal, the heat generation is applied only to those elements lying inside a control box, moving according to the deposition path. The dimensions of such control box are defined according to the layer size, to provide the correct heat input per unit volume, as shown in Eq. (13):

$$V_{el} = lw_l l_l \quad \text{Eq. 13}$$

where w_l is the layer width, h_l is the layer height and l_l is the element size along the deposition direction. Further details of the demonstration are provided in [25].

3.1.2. Material deposition modeling

Another crucial aspect of the AM processes simulation is the material deposition modeling. Indeed, in such technologies the components are created by adding subsequent layers of material. This is usually taken into account by means of specific elements activation algorithms. The FE simulations presented in this paper were carried out using an element activation technique derived from the welding simulation literature. It belongs to the class of quiet element methods, already used to simulate several metal AM processes [28]. In these techniques the elements of the filler material are present during the whole simulation, but their material properties are initially set to specific values that make their contri- bution irrelevant to the global behavior of the structure (e.g., low thermal conductivity and Young's modulus). The material proper- ties are then switched to their actual values when an activation criterion is met. In the models presented in this paper, the activa- tion criterion is based on the elements temperature, as in [29]. Since the initial thermal conductivity is set to a low value, the elements representing the filler metal will undergo a significant tempera- ture increase only when heated by the heat source. Therefore, by setting an activation temperature range, it is possible to switch from the initial to the actual properties values following a linear interpolation function:

$$P(T(\tau)) = \gamma(T_{max})P_{act}\big(T(\tau)\big) + \big(1 - \gamma(T_{max})\big)P_{quiet} \qquad \text{Eq. 14}$$

where P is the generic material property, P_{act} and P_{quiet} its active and quiet values respectively, τ is the current simulation time, $T(\tau)$ is the current element temperature evaluated at the current Gauss point and simulation time while T_{max} is its maximum value experienced by $T(\tau)$, from the simulation start to the current time. The variable γ represent the activation function shown in Fig. 6.

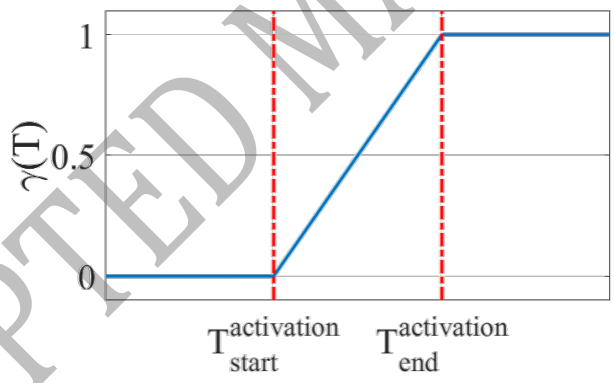

Fig. 6. Activation function.

The temperatures corresponding to the beginning and the end of the activation have been set equal to the solidus and liquidus temperatures respectively.

3.1.3. Latent heat modeling

The last aspect that will be discussed is the latent heat modeling. Indeed, in WAAM and welding simulation, the material behavior at high temperature should be taken into account by means of temperature dependent properties [30]. For the same reason, the latent heat of fusion and solidification should be taken into account, since it significantly raises the actual material heat capacity in the phase transition range. The most common technique adopted in welding and AM simulation is based on artificially raising the value of the temperature dependent heat capacity in the phase transition range in order to cope with the actual material thermal inertia [31]. Despite the fact that this technique is correct from an energetic perspective, the steep heat capacity gradient can impact on the simulation convergence and stability. To overcome this criticality, the latent heat

associated to melting and solidification was treated using a different approach in this work: a heat generation function was defined according to Eq. (15):

$$\dot{q}_{lat} = -\frac{dx_l}{dt}\left(\frac{\rho h_{lat}}{T_l - T_s}\right) \quad \text{Eq. 15}$$

where $\dot{q}_{lat}$ is the generated thermal power per unit volume, ρ is mass density, h_{lat} is the latent heat per unit mass, T_s and T_l are the solidus and liquidus temperatures respectively. The function x_l represents the liquid phase fraction computable according to Eq. (16):

$$x_l = \begin{cases} x_l = 0 & T < T_s \\ x_l = \frac{T - T_s}{T_l - T_s} & T_s \leq T \leq T_l \\ x_l = 1 & T > T_l \end{cases} \quad \text{Eq. 16}$$

It must be pointed out that when the time derivative of the liquid phase fraction is positive (i.e., in material melting) the generated heat will be negative (i.e., it will be subtracted by material internal energy). On the opposite, during the solidification the time deriva- tive of the liquid phase fraction is negative, making the generated heat positive (i.e., added to material internal energy). This results in the same effect of increasing the material heat capacity in the phase transition range.
All the presented techniques have been implemented in the commercial FE solver LS-DYNA: the heat source model was included as a *LOAD HEAT GENERATION [32] and a new material model for thermal analysis was implemented by means of user's subroutines to include the latent heat formulation and the material deposition modeling. For the mechanical simulation the standard LS-DYNA material model dedicated to welding (*MAT CWM [32]) was used. Such material model adopts the presented elements activation strategy.

3.2. Validation models

The test case used for the numerical validation is presented in Fig. 7: it is a single weld bead, deposited onto a square plate substrate.

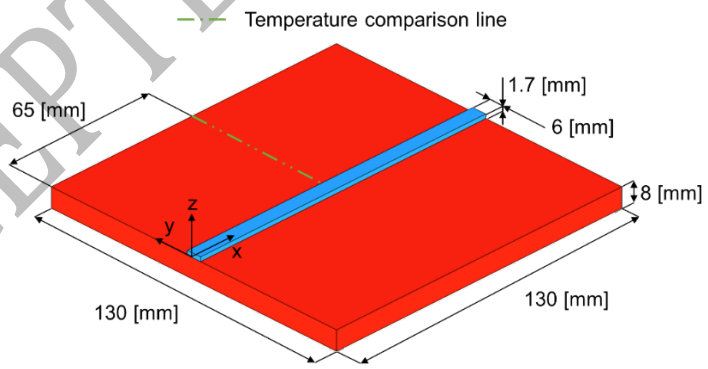

Fig. 7. Geometry of numerical validation models.

The test case model was discretized using both the proposed technique and the mesh biasing approach, in order to compare their performances. A reference model was created discretizing all the substrate with bead mesh size requirements. The accuracy of the FE models was compared analyzing the temperature profile along the comparison line (Fig. 7) at the simulation time in which the heat source was located at x = 65 mm. All the FE simulations were carried out using first order hexahedral elements. Due to the symmetry of the test case, only half of its geometry was discretized: Fig. 8 shows the FE models used in this validation stage.

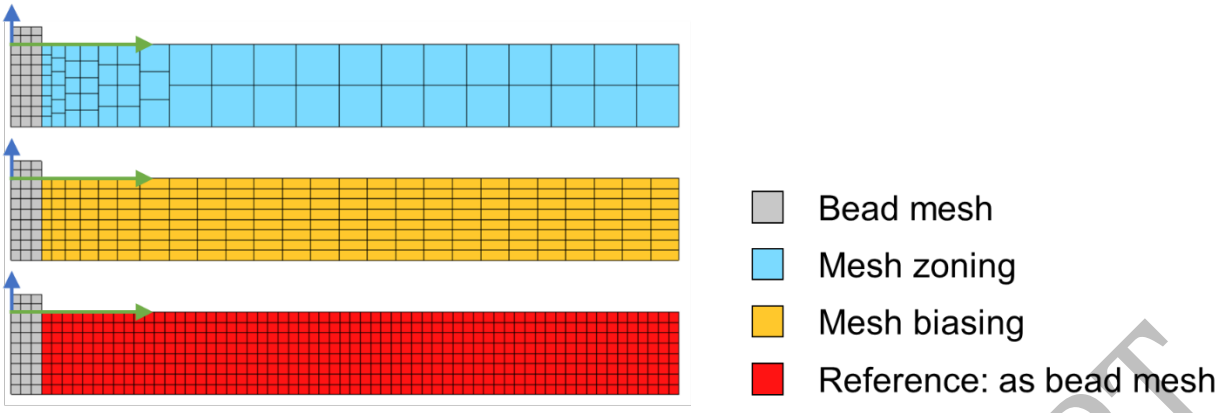

Fig. 8. Comparison of mesh biasing, mesh zoning and reference models.

The proposed model was created setting the maximum error parameter (Err_t) of the proposed mesh size identification algorithm equal to 5%. This led to a FE model composed by 7768 hexahedrons, with a maximum elements aspect ratio not exceeding 1.2. The mesh biasing model was created with the constraint of not exceeding a limit value of the elements maximum aspect ratio (limit value: 3.0), leading to a FE model made of 29900 hexahedrons. In all the FE models, weld bead was discretized with three elements per half width and two elements per thickness. The region underneath the weld bead was discretized using the same mesh size. Follow- ing these guidelines, the reference model was composed by 68380 hexahedrons.
The FE simulation was carried out considering a total heat input per unit time of 2.8e+3 W, and a welding head travelling speed of 300 mm/min. The heat source dimensional parameters were set according to Table 1.

Table 1: Heat source dimensional parameters.

Heat source dimensional parameters [mm]								
a_f	a_r	b	c	f_f	f_r	w_l	h_l	l_l
1,4	3,5	3.0	3.0	0.6	1.4	3.0	1.7	1.44

The material was modelled with thermal property values compliant with a low carbon content mild steel [33]. The material thermal conductivity was artificially raised in the liquid range, according to common welding simulation practices [34]. The inac- tive bead material was modelled scaling the elements thermal conductivity and heat capacity according to the suggestions of Michaleris et al. [8]. The curves of temperature dependent thermal properties used in the simulation for the active material are shown in Fig. 9.

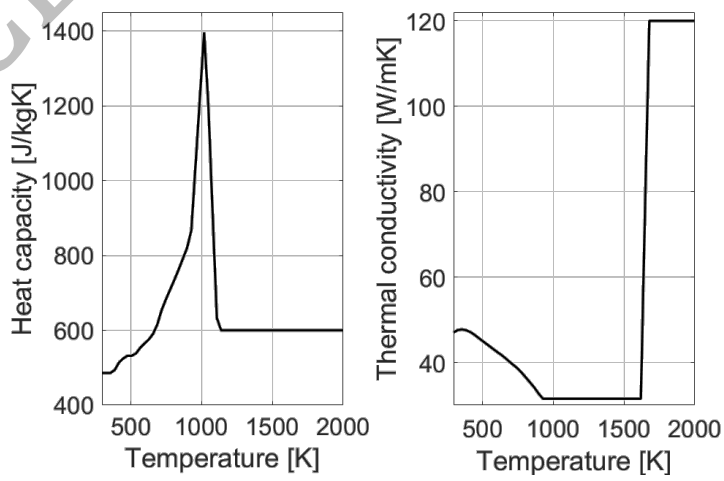

Fig. 9. Temperature dependent material properties curves used in the simulations.

The latent heat of fusion was set to 113.5 kJ/kg, while the solidus and liquidus temperatures were set to 1400° C and 1450° C respec- tively [35]. The simulations were carried out using a Crank-Nicolson time integration scheme, with variable adaptive time stepping [32]. The computations were performed on a PC equipped with an intel core i7 CPU and 16 GB of RAM.
Fig. 10 summarizes the validation results: in Fig. 10a, the temperature profile on the comparison line computed by the reference model is presented. Fig. 10b shows the percentage errors of the mesh biasing and the proposed models with respect to the reference one.

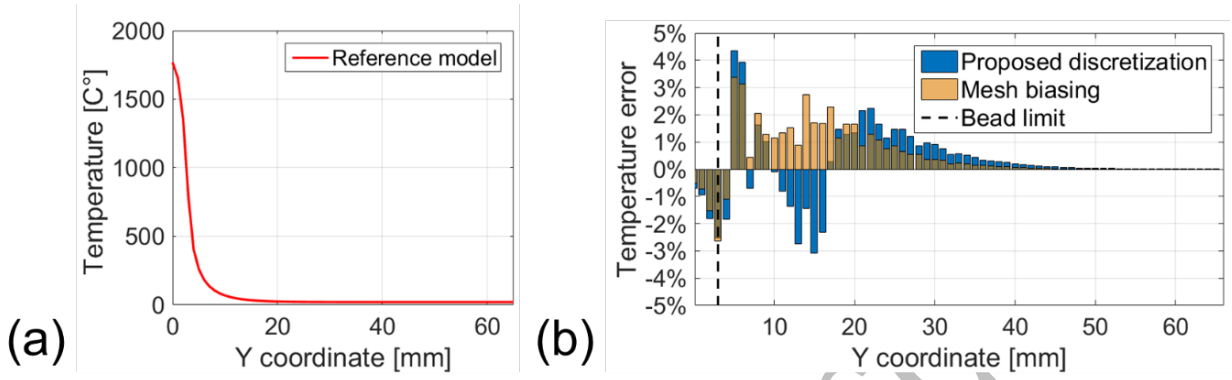

Fig. 10. Reference model temperature profile (a); biased and proposed models error (b).

Fig. 10b clearly highlights that both the element-saving strate- gies lead to reduced percentage errors in estimating the reference temperature profile (below 5%). The mesh biasing model shows a slightly lower error than the proposed one. This might be due to the larger number of elements used to discretize the comparison line in the mesh biased model, as required to meet the maximum aspect ratio constraint. The other aspect to be taken into account is the simulation time: Table 2 compares the elapsed time of the reference, mesh biasing and proposed models. The mesh biasing allowed achieving a great reduction in computational time with respect to the reference one. However, with the proposed model a further improvement was achieved, reducing the computational time of about 70% with respect to the mesh biasing model. This significant difference in simulation time is related to the lower element number used to discretize the proposed model, compared to the mesh biasing one.

Table 2: Simulation times of FE models used in validation analysis

Simulation times [s]		
Reference model	Mesh biasing	Proposed model
26481	10099	3182

In summary, the proposed model returned an accurate prediction of the reference temperature field and allowed to significantly reduce the simulation time. Despite the proposed mesh zoning leads to a slightly larger temperature error with respect to the mesh biasing one, this lack of accuracy might be negligible compared to the great reduction of simulation time provided by the proposed model.

4. Experimental validation

The numerical validation allowed to confirm that the proposed discretization technique returns an accurate prediction of the substrate temperature distribution. As already mentioned, the main purpose of AM simulation is the prediction of workpiece mechan- ical response in terms of distortions and residual stresses. In order to test the effect of the proposed mesh coarsening on the accuracy of mechanical analysis, an experiment was performed. A test-case workpiece was manufactured using the WAAM facility installed in the manufacturing-technologies-research-lab of the University of Firenze. Workpiece distortions were then measured and compared with process simulation results.

4.1. Experiment description

The test case used for the experimental validation is shown in Fig. 11.

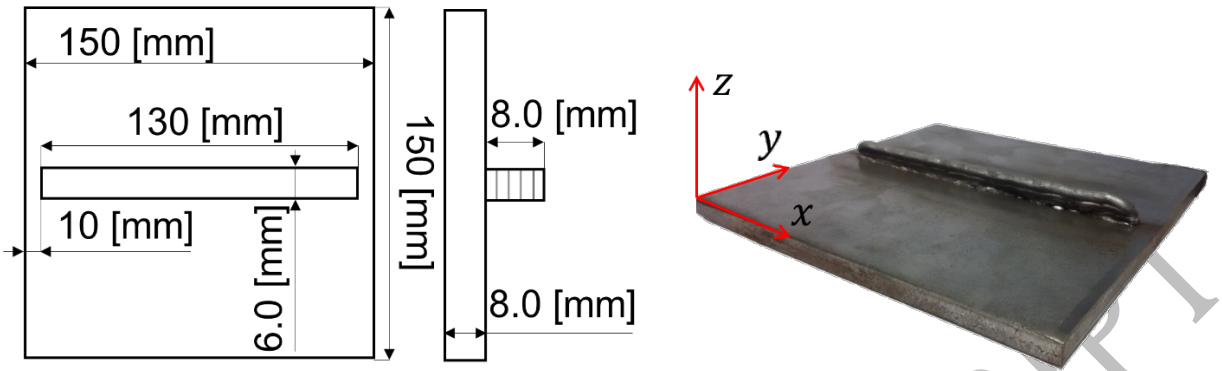

Fig. 11. Test case dimensions and actual appearance.

Basically it consists in a 5 layers wall, i.e., a series of straight beads deposited onto a plane substrate. The substrate is made of S235JR structural steel, while the deposition was carried out using a ER70S-6 0.8 mm metal wire, that is a standard filler material for carbon steel welding. The deposition process was performed using a Millermatic 300 GMAW welding unit, whose torch was fitted onto a purpose built three axis machine tool. The process parameters used for test case manufacturing are summarized in Table 3.

Table 3: Process parameters used to manufacture the test case.

Process parameters	
Average welding voltage	19 [V]
Average welding current	81 [A]
Electrical power	1480 [W]
Wire feed speed	4.6 [m/min]
Travelling speed	300 [mm/min]

The test case was constrained with an isostatic scheme during the deposition process. This fixture scheme was realized supporting the base plate on three rest points. This strategy was preferred to avoid modeling the boundary conditions and the unclamping simulation that could affect the validation analysis. Hence, only the deposition and cooling phases were simulated, without including the unclamping in the FE analysis. The workpiece distortions were measured by means of a Mitutoyo Euro Apex C776 CMM (Coordinate Measurement Machine), probing the top surface of the base plate, i.e., the x-y plane corresponding to z = 0, (Fig. 11). The work- piece was scanned before and after the deposition in order to take into account base plate unevenness in comparing the distortions. The geometry of the FE model top surface was updated projecting the top surface nodes on the actual top surface geometry.

4.2. FE model

The FE modeling of the test case was carried out using the procedures described for the numerical validation models, including the thermal material properties. The substrate discretization was carried out using the proposed technique. The mesh size selection algorithm was run using 10% as maximum error parameter. This lead to a model size of 21742 hexahedrons and 13627 nodes. The mesh coarsening pattern is shown in Fig. 12.

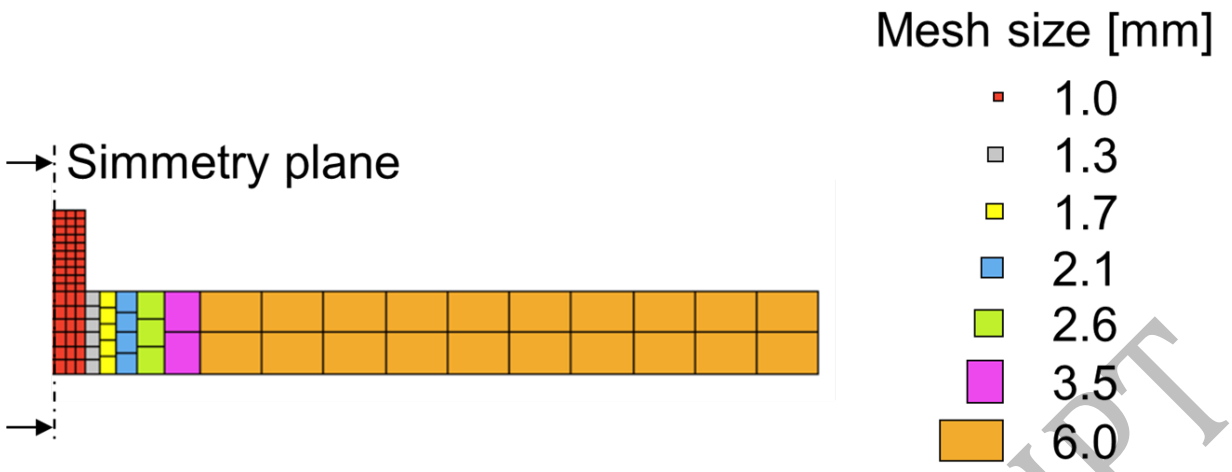

Fig. 12. Mesh size pattern for the wall model.

The weld beads were discretized using three elements per half bead width and two elements in the arc aiming direction. The heat source dimensional parameters were set according to the values used for the numerical validation.

For the heat transfer analysis, free convection Boundary Conditions (BCs) were assigned on the substrate top and bottom surfaces and on the wall surface, with heat transfer coefficients equal to 8.5W/(m^{2}K), 4.0 W/(m^{2}K), 12.0 W/(m^{2}K) respectively. The heat transfer coefficients were computed using literature correlations for free convection [36]. A general radiation to environment BC was included, setting the material emissivity to 0.2 [37]. For both the convection and radiation BCs, the room temperature was set to 298.16 K.

From the mechanical perspective, the solution was performed using a fully implicit integration scheme. Since in LS-DYNA the mechanical and heat transfer analyses are carried out by different solvers using different simulation steps, mechanical and thermal time step were forcedly synchronized as in [32]. Literature curves [33], shown in Fig. 13, were employed to take into account the temperature dependency of the material mechanical properties. The thermal properties were set as described in Section 3.2.

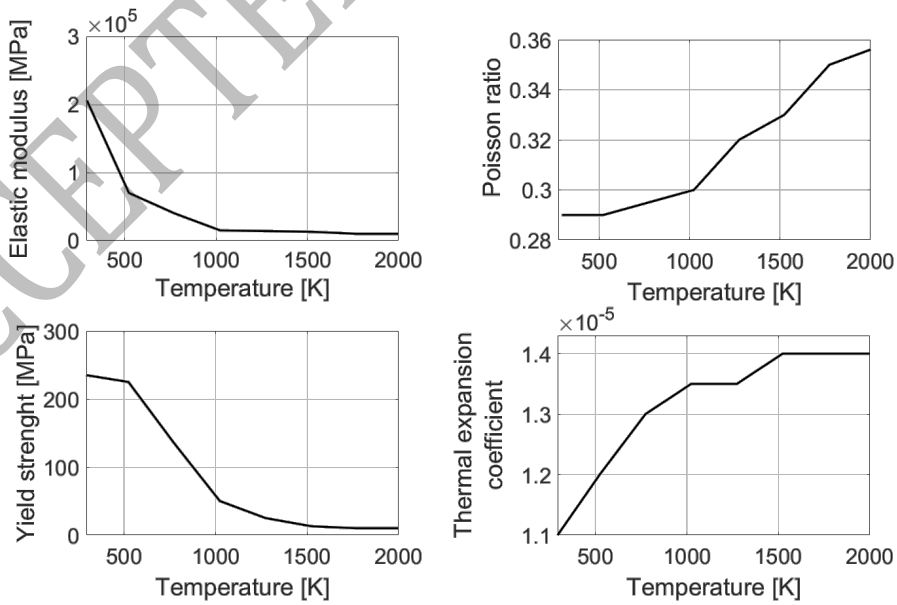

Fig. 13. Material mechanical properties used for the wall manufacturing simulation.

As mentioned, the mechanical behavior of the filler material was modelled using the LS-DYNA embedded material model *MAT CWM that allows managing the elements activation with the quiet element method. The activation start and end temperatures were set according to the numerical

validation model, while ghost values for the mechanical properties were set to be 1E-5 times the maximum value of each property in the analysis temperature range. The mechanical boundary condition was modelled introducing single point constraints in correspondence of the rest points. The retained DOFs were selected to achieve an isostatic scheme, as in the actual manufacturing process.

4.3. Results analysis

The prediction accuracy of the workpiece mechanical response was evaluated comparing the deformed top surface of the actual plate and the simulated one. In Fig. 14 the experimental and simulated surfaces are compared.

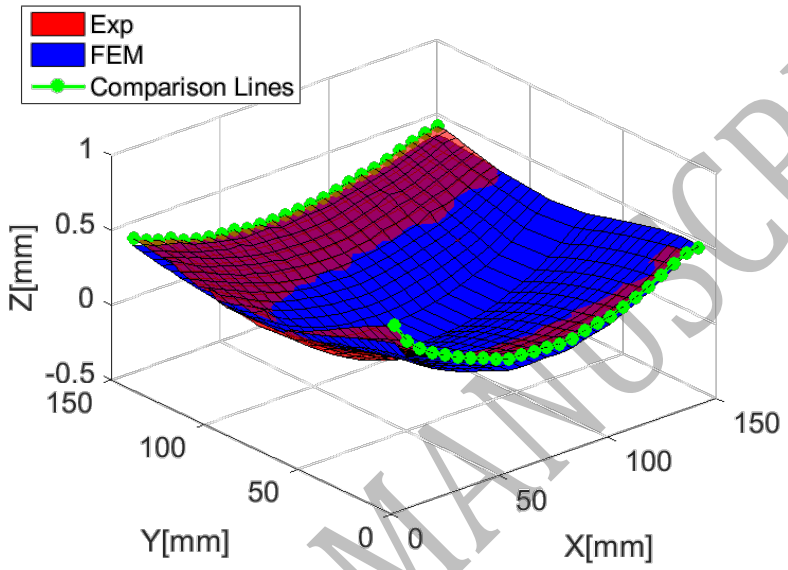

Fig. 14. Predicted and experimental top surface deformed geometry.

To provide a better insight on the simulation accuracy, the two edges of the top surface in the X direction (green lines with round markers in Fig. 14) are shown separately in Fig. 15.

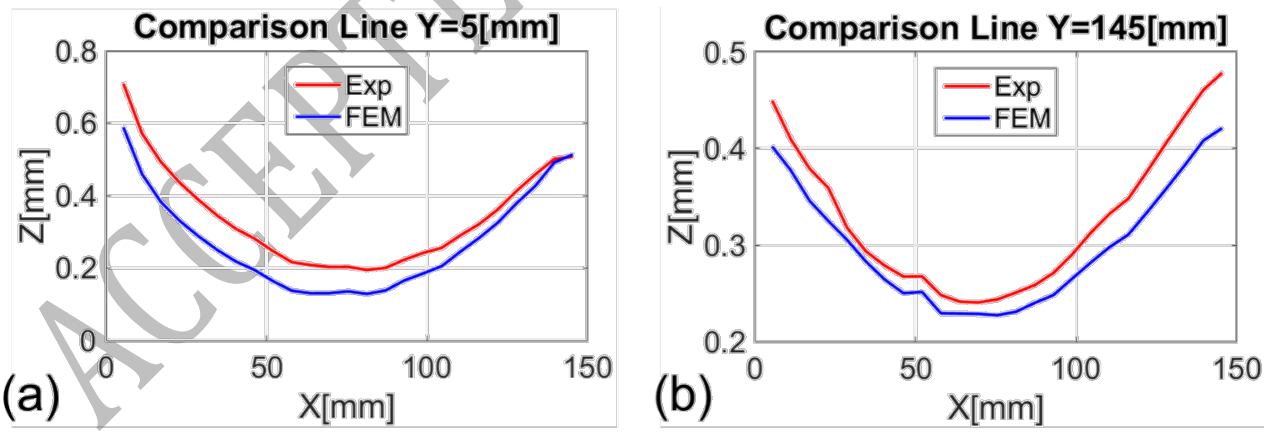

Fig. 15. Predicted and experimental comparison lines.

As shown in the figures, FE simulations results are in general agreement with the experimental ones. Indeed, the surface curvature are quite similar, with a maximum error of 0.16 mm on the z position. This result is in line with what presented in previous works concerning WAAM simulation [10,14]. This level of accuracy allows to effectively adopt process simulation for the optimization of process parameters and the development of distortion mitigation strategies. Furthermore, the simulation was carried out using literature data and correlations for material properties and heat transfer coefficients and without any model updating operations to identify the heat source parameters. This suggests

that the simulation accuracy could be improved with a better estimate of the input parameters. In summary, the simulation carried out by means of the proposed discretization techniques allows to achieve an accuracy level compliant with literature data, for what concerns workpiece distortions, confirming the results obtained in the numerical validation.

5. Conclusions

This paper presents a new procedure aiming at reducing the computational time of WAAM simulation. Such technique is based on reducing the number of elements required to discretize the substrate, thanks to a mesh zoning procedure. The technique is based on two key aspects: the mesh size definition and the mesh zones joining. The substrate is divided into zones, discretized without the conformable interfaces mesh constraint. The zones are then merged through double sided thermo-mechanical contact. The mesh zones sizes were defined using a pre-process algorithm developed to identify the mesh size pattern that ensures a target level of interpolation accuracy. This allows to define a mesh pattern consistent with the expected temperature distributions, balancing the modeling accuracy and computational efficiency. At the same time, the usage of double sided contact algorithm strongly limits the occurrence of issues related to high aspect ratio elements.
The proposed technique was validated by means of a two-step approach. For starters, a numerical test case was used to compare the proposed technique with the traditional mesh biasing approach, in terms of simulation time and temperature distribution accuracy. This validation showed the effectiveness of the proposed technique, proving that it can return accurate predictions of work-piece temperature field, with respect to a reliable reference model, while significantly reducing the process simulation time.
In addition, an experimental validation was carried to verify whether the accuracy of the proposed technique, in terms of temperature distribution prediction, resulted in an accurate prediction of workpiece mechanical response as well. A simple test-case was manufactured, measuring its distortions. The manufacturing process was simulated according to the proposed technique, comparing the simulated and measured distortions. The validation analysis highlighted that the proposed FE model was capable of predicting the workpiece distortions, meeting the standard accuracy of state of the art WAAM simulation models. Furthermore, such goal was achieved without performing any model updating operations on the material proprieties, BCs or heat source parameters, confirming that the proposed substrate meshing strategy allows to achieve an adequate trade-off between accuracy and computational efficiency.
In conclusion, the proposed technique represents a systematic effective tool, guiding the pre-processing phase of WAAM FE models.

References

[1] C. V Haden, G. Zeng, F.M. Carter, C. Ruhl, B.A. Krick, D.G. Harlow, Wire and arc additive manufactured steel: Tensile and wear properties, Addit. Manuf. 16 (2017) 115–123. doi:10.1016/j.addma.2017.05.010.

[2] M. Liberini, A. Astarita, G. Campatelli, A. Scippa, F. Montevecchi, G. Venturini, M. Durante, L. Boccarusso, F.M.C. Minutolo, A. Squillace, Selection of Optimal Process Parameters for Wire Arc Additive Manufacturing, Procedia CIRP. 62 (2017) 470–474. doi:10.1016/j.procir.2016.06.124.

[3] K.F. Ayarkwa, S.W. Williams, J. Ding, Assessing the effect of TIG alternating current time cycle on aluminium wire + arc additive manufacture, Addit. Manuf. 18 (2017) 186–193. doi:10.1016/j.addma.2017.10.005.

[4] F. Montevecchi, G. Venturini, N. Grossi, A. Scippa, G. Campatelli, Finite Element mesh coarsening for effective distortion prediction in Wire Arc Additive Manufacturing, Addit. Manuf. 18 (2017) 145–155. doi:10.1016/j.addma.2017.10.010.

[5] A. Addison, J. Ding, F. Martina, H. Lockett, S. Williams, Manufacture of Complex Titanium Parts using Wire + Arc Additive Manufacture, in: Titan. Eur. 2015, 2015.

[6] D. Ding, Z. Pan, D. Cuiuri, H. Li, A tool-path generation strategy for wire and arc additive

manufacturing, Int. J. Adv. Manuf. Technol. 73 (2014) 173–183. doi:10.1007/s00170-014-5808-5.
[7] D. Ding, Z. Pan, D. Cuiuri, H. Li, N. Larkin, Adaptive path planning for wire-feed additive manufacturing using medial axis transformation, J. Clean. Prod. 133 (2016) 942–952. doi:10.1016/j.jclepro.2016.06.036.
[8] J. Kao, F.B. Prinz, Optimal Motion Planning for Deposition in Layered Manufacturing, 1998 ASME Des. Eng. Tech. Conf. (1998) 10.
[9] Y. Nilsiam, P. Sanders, J.M. Pearce, Slicer and process improvements for open-source GMAW-based metal 3-D printing, Addit. Manuf. 18 (2017) 110–120. doi:10.1016/j.addma.2017.10.007.
[10] Y. Cao, S. Zhu, X. Liang, W. Wang, Overlapping model of beads and curve fitting of bead section for rapid manufacturing by robotic MAG welding process, (2011). doi:10.1016/j.rcim.2010.11.002.
[11] J. Xiong, G. Zhang, H. Gao, L. Wu, Modeling of bead section profile and overlapping beads with experimental validation for robotic GMAW-based rapid manufacturing, Robot. Comput. Integr. Manuf. 29 (2012) 417–423. doi:10.1016/j.rcim.2012.09.011.
[12] D. Ding, Z. Pan, D. Cuiuri, H. Li, A multi-bead overlapping model for robotic wire and arc additive manufacturing (WAAM), Robot. Comput. Integr. Manuf. 31 (2015) 101–110. doi:10.1016/j.rcim.2014.08.008.
[13] J. Mehnen, J. Ding, H. Lockett, P. Kazanas, Design study for wire and arc additive manufacture, Int. J. Prod. Dev. 19 (2014) 2. doi:10.1504/IJPD.2014.060028.
[14] G. Venturini, F. Montevecchi, A. Scippa, G. Campatelli, Optimization of WAAM Deposition Patterns for T-crossing Features, in: Procedia CIRP, 2016: pp. 95–100. doi:10.1016/j.procir.2016.08.043.
[15] H.L. Lockett, M.D. Guenov, Graph-based feature recognition for injection moulding based on a mid-surface approach, CAD Comput. Aided Des. 37 (2005) 251–262. doi:10.1016/j.cad.2004.06.010.
[16] S. Subrahmanyam, M. Wozny, An overview of automatic feature recognition techniques for computer-aided process planning, Comput. Ind. 26 (1995) 1–21. doi:10.1016/0166-3615(95)80003-4.
[17] S. Davidson, Grasshopper (Algorithmic modeling for Rhino), (2015). http://www.grasshopper3d.com/ (accessed March 14, 2018).
[18] Robert McNeel & Associates, Rhinoceros 5 for Windows User's Guide, 2016. http://docs.mcneel.com/rhino/6/usersguide/en-us/windows_pdf_user_s_guide.pdf (accessed March 14, 2018).
[19] SDK openNURBS, (n.d.). https://www.rhino3d.com/opennurbs (accessed March 14, 2018).
[20] E.A. Nasr, A.K. Kamrani, Computer-Based Design and Manufacturing Computer-Based Design and Manufacturing, 2007. http://www.springerlink.com/content/n2574k72123p2g24/abstract/.
[21] E. Reid, G. Morea, D. a. Harrod, A. Peltzman, C. Parks, W.B. Gruttke, The Initial Graphics Exchange Specification (IGES) Version 5.x, (2006) 1--754.
[22] A.K. Kamrani, E.A. Nasr, Rapid Prototyping: Theory and Practice, 2006. doi:10.1039/c1lc20514e.
[23] S. Jhavar, N.K. Jain, C.P. Paul, Development of micro-plasma transferred arc (□ -PTA) wire deposition process for additive layer manufacturing applications, J. Mater. Process. Tech. 214 (2014) 1102–1110. doi:10.1016/j.jmatprotec.2013.12.016.
[24] A. Adebayo, Characterization of integrated WAAM and machining process, Cranfield University, 2013.
[25] X. Li, H. Jiang, S. Chen, X. Wang, An efficient surface – surface intersection algorithm based on geometry characteristics, Comput. Graph. 28 (2004) 527–537. doi:10.1016/j.cag.2004.04.008.
[26] J. Xiong, Z. Yin, W. Zhang, Forming appearance control of arc striking and extinguishing area in multi-layer single-pass GMAW-based additive manufacturing, Int. J. Adv. Manuf. Technol. 87 (2016) 579–586. doi:10.1007/s00170-016-8543-2.
[27] A.A. Ugla, O. Yilmaz, Deposition-Path Generation of SS308 Components Manufactured by TIG Welding-Based Shaped Metal Deposition Process, Arab. J. Sci. Eng. (2017).

doi:10.1007/s13369-017-2582-3.
[28] J. Mehnen, J. Ding, Design study for wire and arc additive manufacture, X (n.d.).
[29] F. Montevecchi, G. Venturini, N. Grossi, A. Scippa, G. Campatelli, Idle times selection for wire-arc-additive-manufacturing: a finite element based technique, Addit. Manuf. (2018).
[30] F. Montevecchi, G. Venturini, A. Scippa, G. Campatelli, Finite Element Modelling of Wire-arc-additive-manufacturing Process, in: Procedia CIRP, 2016: pp. 109–114. doi:10.1016/j.procir.2016.08.024.